PNAS RESEARCH ARTICLE | ENGINEERING
BIOPHYSICS AND COMPUTATIONAL BIOLOGY

Walking is like slithering: A unifying, data-driven view of locomotion

Dan Zhao[a,b], Brian Bittner[a,c,d], Glenna Clifton[e], Nick Gravish[f], and Shai Revzen[a,g,h,1]

Edited by Robert Full, University of California, Berkeley, CA; received October 16, 2021; accepted August 4, 2022 by Editorial Board Member Klavs F. Jensen

Legged movement is ubiquitous in nature and of increasing interest for robotics. Most legged animals routinely encounter foot slipping, yet detailed modeling of multiple contacts with slipping exceeds current simulation capacity. Here we present a principle that unifies multilegged walking (including that involving slipping) with slithering and Stokesian (low Reynolds number) swimming. We generated data-driven principally kinematic models of locomotion for walking in low-slip animals (Argentine ant, 4.7% slip ratio of slipping to total motion) and for high-slip robotic systems (BigANT hexapod, slip ratio 12 to 22%; Multipod robots ranging from 6 to 12 legs, slip ratio 40 to 100%). We found that principally kinematic models could explain much of the variability in body velocity and turning rate using body shape and could predict walking behaviors outside the training data. Most remarkably, walking was principally kinematic irrespective of leg number, foot slipping, and turning rate. We find that grounded walking, with or without slipping, is governed by principally kinematic equations of motion, functionally similar to frictional swimming and slithering. Geometric mechanics thus leads to a unified model for swimming, slithering, and walking. Such commonality may shed light on the evolutionary origins of animal locomotion control and offer new approaches for robotic locomotion and motion planning.

locomotion | slipping | walking | slithering | low Reynolds number

Significance

Animals move by generating forces against their surrounding environment. We present a unifying framework that applies to slithering, walking, and swimming in viscous (Stokes) fluids. Our results show the kinematic term from the reconstruction equation of geometric mechanics, previously known to govern slithering and Stokesian swimming, applies to multilegged walking animals (ants) and robots, both with and without slipping. We describe procedures for building principally kinematic models from observations and for testing their validity. This provides a universal model for locomotion that applies whenever the movement is dominated by continuous friction with the environment. The universality of this approach may have application in robot design and motion planning and provide insight into the evolution and control of legged locomotion.

Locomotion in living systems is typically characterized by periodic movements of appendages and body elements that propel organisms through the world. It is often observed that the forward speed of an animal is linearly related to the frequency of body movements (1). For example, walking insects (2–4), crawling worms (5, 6), slithering reptiles (7–9), and swimming microorganisms (10, 11) all exhibit such relationships. However, there are notable exceptions as well; for example, birds and fish can soar or glide over a range of speeds while their body oscillation frequency is zero. The distinction to be made between these observations is the importance of momentum. Soaring birds and gliding fish are capable of building up momentum to decouple body undulation from forward speed. However, organisms that move through viscous fluids, or those that slip producing ongoing high friction, dissipate their momentum very quickly.

Within environments where friction forces are large the body velocity v is linearly dependent on the rate of body shape change $\dot{r}$ through multiplication by a shape-dependent matrix $A(r)$, giving the equation $v_b = A(r)\dot{r}$. Motion through these environments is often referred to as "Stokesian" because it is most familiar from the literature on swimming in low Reynolds numbers fluids, which are often called "Stokes flows" (12). An early observation of such an instantaneous relationship appears in Purcell's swimming model from his seminal paper "Life at low Reynolds number" (13). Shapere and Wilczek (14) derived this relationship for more general viscous swimming using tools from differential geometry. With the growing interest in granular media and their similarity to fluids, new experiments observed similar phenomena in undulatory locomotion on and within sand (15–20). A particular surprise in granular media was that this shape-dependent, linear relationship between body velocity v and shape velocity $\dot{r}$ arose despite the fact that interaction forces between body and granular media are velocity independent, while in Stokes flows this relationship arose in an obvious way from linear viscosity (13).

A key result in the development of Stokesian motion models was the insight, rigorously formalized by Hatton and Choset in ref. 21, that with an appropriate choice of body frame the optimality of a Stokesian gait for a body with two degrees of freedom (DoF) can be determined from the level set of a scalar height function. This extends to optimal swimming under other fluid interaction models (22) and can be generalized to optimization of motion with bodies that have more than two DoF (23). It is in a collaboration with this group that we created the tools for data-driven identification of Stokesian motion models (24, 25) we use in the current paper.

Author contributions: D.Z., G.C., B.B., N.G., and S.R. designed research; D.Z. designed the robots; D.Z., G.C., and S.R. performed research; D.Z. performed robot experiments; G.C. built the ant experimental setup; G.C. collected ant data; D.Z. and B.B. analyzed data; D.Z. performed robot analysis; N.G. supervised ant work; S.R. supervised robot work; S.R. provided theoretical background; and D.Z., B.B., G.C., N.G., and S.R. wrote the paper.

The authors declare no competing interest.

This article is a PNAS Direct Submission. R.F. is a guest editor invited by the Editorial Board.

Copyright © 2022 the Author(s). Published by PNAS. This article is distributed under Creative Commons Attribution-NonCommercial-NoDerivatives License 4.0 (CC BY-NC-ND).

[1]To whom correspondence may be addressed. Email: shrevzen@umich.edu.

This article contains supporting information online at https://www.pnas.org/lookup/suppl/doi:10.1073/pnas.2113222119/-/DCSupplemental.

Published September 6, 2022.

Downloaded from https://www.pnas.org by UNIVERSITY OF CALIFORNIA DIGITAL LIBRARY CDL ACQUISITIONS GEISEL LIBRARY on September 12, 2022 from IP address 128.54.25.186.

Historically, geometric mechanics models with no momentum terms were developed in the context of Stokes fluids and extended to highly dissipative granular media. Thus, the term Stokesian applies to both low Reynolds number swimming and slithering on granular media. However, in both of these locomotion regimes, drag resists momentum at all locations along the body and at all times, setting up an expectation of continuous momentum dissipation for any geometric mechanics model termed Stokesian. In this paper, we show that geometric mechanics models also apply to legged systems that only encounter resistance at discrete contact points with the ground. To avoid a connotation of continuous drag, we use the more verbose technical term "principally kinematic" for the systems we consider (also used in ref. 26).

While geometric mechanics has been applied to legged systems, it has primarily relied on nonslip contacts or the availability of explicit force-based models of the contact physics. Some of the earliest work on legged systems was done by Kelly and Murray (27), who provided an example based on a no-slip hexapedal robot. Goodwine and Burdick (28) proposed methods of motion planning for kinematic stratified systems, a class that includes multilegged motion. Although they do mention the possibility of slipping,* their paper focuses on the stratified structures themselves and is predicated on contact models being available. The extension of this theoretical work to empirical systems was first performed studying salamander walking on granular media (15). Subsequent work from the same group has applied principally kinematic locomotion models in designing and analyzing walking gaits, on both granular surfaces (29) and solid frictional substrates (30, 31), while allowing foot contacts to slip and thus extending beyond the early nonslip theoretical work discussed above. A critical feature of all these studies is that they 1) involved an exhaustive scan of possible shapes and motions which would be infeasible in high-dimensional shape spaces, 2) relied on a model of the foot–ground contact forces, and 3) critically relied on reducing the high DoF shape spaces of robots and animals to two DoF shape spaces, to enable both the optimization and experimental analysis in those studies.

The key contribution of our paper is demonstrating that principally kinematic models extend to high DoF shape spaces and that the principal kinematic relationship $v_b = A(r)\dot{r}$ can be validated for animals and robots without assumptions on the foot–ground contact model. In particular, we 1) expand the application of the term principally kinematic to a broad class of walking systems where friction is sufficiently high to produce a locomotion model of $v_b = A(r)\dot{r}$; 2) illustrate that principally kinematic equations of motion arise naturally in nonslip walking and appear in multilegged walking with slipping; 3) record and track walking kinematics of ants and two classes of multilegged robots producing data for high DoF shape space systems; 4) use efficient data-driven methods to identify that principally kinematic models are excellent predictors for walking without slipping (ants) and with substantial slipping (robots); and 5) test the empirically generated models by predicting behaviors outside the training data, demonstrating their ability to be used for control, motion planning, and optimization or learning. Our results combined with prior work on swimming, slithering, and walking reveal the generality of principally kinematic models and suggest that they should play a more central role in the investigation of legged locomotion for kinesthetic learning, evolution, and robotic planning or control.

*This appears in ref. 28, p. 217.

Background

Here we establish the rationale for modeling both nonslip and slipping walking as principally kinematic motion. We define locomotion as the change of a body-attached coordinate frame through the world over time. In the following subsections we will distinguish between the kinematic modes of walking using concepts from geometric mechanics and rigid body transformations (for a concise refresher, see ref. 32).

When Legs Are Planted, the Motion Is Principally Kinematic. Consider the motion of a legged animal or robot with respect to a nonslip, irrotational contact. In such a case, there is a map $g = F(r),\ F : \mathcal{Q} \to \mathsf{SE}(3)$ from the body shape $r \in \mathcal{Q}$ taken from space of possible body shapes $\mathcal{Q}$, to the location of and orientation of the body frame with respect to a frame attached to the contact feet and therefore attached to the world frame. The body frame is represented by a rigid body transformation, g. Here g is a member of the standard Euclidean group of rigid body transformations $\mathsf{SE}(3)$, represented as matrices. This kind of motion is called "holonomic" because it arises from the whole function F. As a consequence of being holonomic, no periodic motion in r can lead to a net average motion through the world because when r returns to its initial value, g also returns to its initial value.

Although no average motion is possible without breaking contact with the environment, holonomic segments of motion provide an important insight: they show that a body velocity can be written in a principally kinematic form by differentiating $g = F(r)$ to give $\dot{g} = J_F(r)\dot{r}$ with J_F the Jacobian of the map F and $\dot{g}$ the body velocity written with respect to the world frame. It is natural to rewrite the body velocity with respect to the body frame, given by taking $A_F(r) := (F(r))^{-1}J_F(r)$, obtaining that $v_b := g^{-1}\dot{g} = A_F(r)\dot{r}$. This form is the local connection appearing as the fiber bundle form of principally kinematic motion described in many sources (12, 14, 21, 24, 33). For each shape $r \in \mathcal{Q}$, $A_F(r) : \mathsf{T}_r\mathcal{Q} \to \mathfrak{se}(3)$ maps the space of possible body shape change velocities $\mathsf{T}_r\mathcal{Q}$ at the shape r to the space of body velocities in the body frame of reference, which is the Lie algebra $\mathfrak{se}(3)$.

Legged Locomotion without Slipping Is Always Principally Kinematic. As a legged animal or robot moves through the world without slipping, legs are necessarily planted and detached from the environment. For every fixed set of contacts with the environment $c \in C$, taken from a finite set of possible contact combinations C, there exists a holonomic $F[c] : \mathcal{Q} \to \mathsf{SE}(3)$. As noted previously, if the same set of planted contacts remains, no motion is possible. As feet are lifted off the ground and other feet are placed, the set of contacts c with respect to which $F[c]$ is written undergoes discrete changes. When the set of contacts changes, this can give a jump in the body frame relative to the feet.† However, both the body velocity v_b and the change in shape $\dot{r}$ are expected to be continuous. Assuming for simplicity that the set of contacts c is a function of the body shape r, the function $A(r) := A_{F[c(r)]}(r)$ is potentially discontinuous where $c(r)$ changes value but leads to a principally kinematic model for nonslip multilegged locomotion $v_b = A(r)\dot{r}$. Crucially, this $A(\cdot)$ cannot be generated from the Jacobian of any one function $F(\cdot)$. It is not holonomic; it is only piecewise holonomic. Because it is not holonomic, there is room for cyclic shape changes to produce

†In general, $F[c_1](r) \neq F[c_2](r)$ even for shapes, i.e., r values, where c_1 can switch to c_2, i.e., the set of contacts can change.

Downloaded from https://www.pnas.org by UNIVERSITY OF CALIFORNIA DIGITAL LIBRARY CDL ACQUISITIONS GEISEL LIBRARY on September 12, 2022 from IP address 128.54.25.186.

net locomotion. Such piecewise approaches to developing $A(r)$ in multilegged walking have recently been demonstrated in, e.g., ref. 29.

Inertial Systems Can Be Principally Kinematic. It should be noted that the presence of inertial and dynamic effects on the shape of the body does not necessarily stop a motion from being principally kinematic. In the examples above where feet are planted without slip (*When Legs Are Planted, the Motion Is Principally Kinematic* and *Legged Locomotion without Slipping Is Always Principally Kinematic*) the system is (piecewise) holonomic, and the rigid body transformation g which relates the body frame to the world frame is a function of body shape r; i.e., there exists a function $g = F(r)$. As long as this function exists, i.e., all relevant shape variables are knowable and together they determine g, we can differentiate this function to get the body velocity with respect to shape, independent of whether elastic or inertial effects act on the system to create the particular r. In other words, as long as the shape r is a complete intermediate variable in the causal chain between the dynamics and the body's motion in space, the motion can be principally kinematic. Whether the motion is inertial or not does not come into play.

Statically Unstable Systems Can Be Principally Kinematic. To be principally kinematic, a system must obey $v_b = A(r)\dot{r}$ for the domain of r and $\dot{r}$ values which it exhibits. It follows that the body motion covaries with the shape change so as to make the net motion depend only on the shape of the r trajectory and not on its rate. This, however, does not require that the domain of the principally kinematic model extend to all values of $\dot{r}$, including being zero. Being principally kinematic is a property of a behavior, and that behavior might not include standing in place. As long as the position of the body frame is completely determined by the shape changes, these motions are still principally kinematic.

Slipping Can Be Principally Kinematic as Well. While nonslip legged locomotion is often piecewise holonomic, when feet slip, the motion might no longer be holonomic. If the sliding foot contacts generate sufficient friction to quickly dissipate any momentum the body has, the motion becomes principally kinematic. This follows from taking the reduced equations of motion (ref. 33, equation 2.5) at the limit $p \to 0$. The mathematical result would not be too far different from the description of whole-body linear friction as appearing in low Reynolds number swimming and in snake slithering (34), despite having arisen from a rate-independent Coulomb friction.

Summary: Principally Kinematic Models Could Be of Broad Applicability to Legged Locomotion. The aforementioned derivations suggest that although principally kinematic motion models have been studied extensively in low Reynolds number swimming and undulatory movement on frictional surfaces, they may have broad application to legged locomotion. For nonslip locomotion, they have lurked, hidden from view by a simple mathematical derivation. However, they may also apply to legged locomotion with slipping. Discovering whether that is in fact the case in experimental systems is the focus of the remainder of this paper.

Approach

Our purpose is to determine whether an observed legged system is principally kinematic. We employed two methods to assess this: 1) directly estimating the local kinematic connection $A(\cdot)$ to validate the instantaneous behavior expected in principally kinematic motion and 2) evaluating whether the motion is exhibiting the averaged features expected of principally kinematic motion, in particular with regard to gait frequency changes.

To construct our models we collected shape measurements and body motion from high-speed video motion tracking in ants (Argentine ants, *Linepithema humile*), a six-legged robot (BigANT), and a family of multilegged robots (Multipod) with leg numbers ranging over 6, 8, 10, and 12 (see Fig. 1).

Instantaneous Analysis: Estimating the Connection. The most direct way to test for principally kinematic motion is to estimate and validate the local kinematic connection $A(\cdot)$. Here the question is whether body velocity v_b can be determined by a model of the form $v_b = A(r)\dot{r}$, where $r \in \mathcal{Q}$ is the body shape, and the body velocity $v_b := g^{-1}g \in \mathfrak{se}(3)$ is derived from observed body positions and orientations $g \in \mathsf{SE}(3)$. Since the systems in question are noisy, the values of r never recur in the data, and so we must choose some function approximation scheme for $A(\cdot)$ and justify its validity based on noisy observations of g and r. We employed the method described in detail in refs. 24 and 35 and summarized briefly here.

The general nonlinear dependence of $A(r)$ on r would render our estimation attempts futile were it not for the periodic gaits usually employed by animals and robots. Periodic gaits are cyclic changes in body shape that generate a net motion through the world. This cyclic behavior allowed us to reinterpret the collection of observed shapes as a phase $\theta \in \mathcal{Q}$ within the cycle and an offset δ from the typical shape at that phase, breaking down r as $r = \theta + \delta$. The merit of this decomposition is that δ is small, and θ only occupies a one-dimensional space of possible values. By selecting a body frame $g \in \mathsf{SE}(3)$ in the tracking data, we obtained cyclic foot motions with respect to the body and used these to estimate the phase θ using the *phaser* algorithm (36). We also differentiated (two-sample finite difference) the foot motions to obtain $\dot{\theta}$ and $\dot{\delta}$. The resulting dataset consisted of tuples $(g, \theta, \delta, g^{-1}\dot{g}, \dot{\theta}, \dot{\delta})$. As in ref. 24, we expanded $A(r)\dot{r} = A(\theta + \delta)(\dot{\theta} + \dot{\delta})$ using a Taylor series expansion around the point $(\theta, \dot{\theta}) \in \mathsf{T}\mathcal{C}$ and then estimated the terms of this expansion by linear regression. Additional details can be found in section 5.2 of ref. 24.

Our goal was to assess the value of a principally kinematic model as a minimalistic prediction of body velocity in multilegged locomotion. As our metric for comparing the predictive quality of models, we used the ratio of root-mean-square error (RMSE) prediction errors $(1 - \mathrm{RMSE}_1/\mathrm{RMSE}_0)$ of the model RMSE_1 and the baseline model RMSE_0 being compared to. This is similar to the familiar $\mathbf{R}^2$ value used in linear regression. A 100% prediction quality indicates a perfect prediction, a 0% prediction did not reduce the error at all compared to the baseline model being compared to, and a 50% prediction had half the RMSE error of the baseline model.

We also wished to assess the domain of validity of the principally kinematic models we produced. To accomplish this we constructed the models for a restricted behavioral category (e.g., moderate speed with no turning) and tested their ability to predict the outcomes of behaviors outside this behavioral category (e.g., fast motion turning to the right). Such ability to extrapolate is critical if these principally kinematic models are to be usable for design and optimization of robot behaviors.

Since we were seeking a minimal model, we compared our principally kinematic prediction with a simpler model: body

Downloaded from https://www.pnas.org by UNIVERSITY OF CALIFORNIA DIGITAL LIBRARY CDL ACQUISITIONS GEISEL LIBRARY on September 12, 2022 from IP address 128.54.25.186.

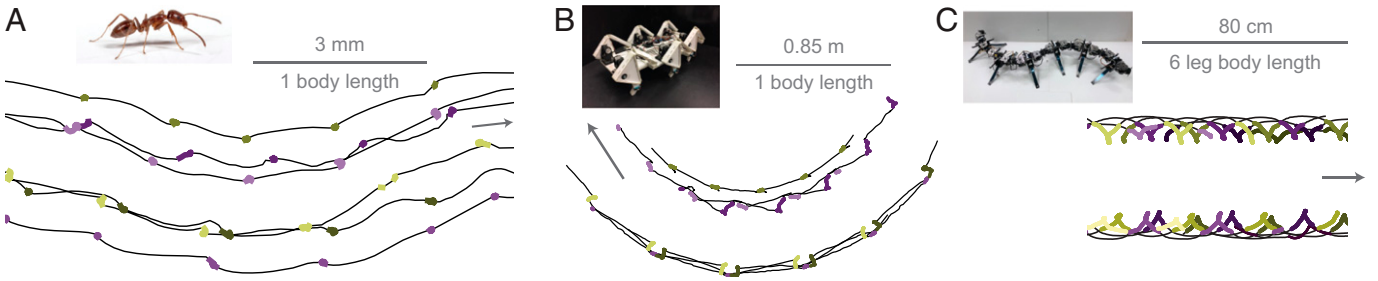

Fig. 1. Foot motions through space for ants and two robots. We highlighted (thick colored lines) the feet when in stance. For animals, we assumed stance when the foot was moving backward with respect to the body. For robots, we assumed stance when the tip of a foot was close to the ground. (*A*) Ants barely slip. (*B*) BigANT slips a moderate amount (18.8% slip ratio). (*C*) The 12-legged Multipod slips much more (51.0% slip ratio). All of these can be represented well by a principally kinematic model.

velocity as a function of phase alone, represented as a Fourier series $v_{\text{fs}}(\theta)$. However, because we tested for model extrapolation across speeds, this very simple alternative would have been unfairly disadvantaged. To allay this concern, we also considered a shape velocity alternative: body velocity being as a function of phase alone, rescaled by a ratio of the average rates of shape change. For each trial k, we computed the average shape change speed $s_k := \text{average}_t(\|\dot{r}(t)\|)$. This model prediction for an animal or robot at phase θ of trial k was $(s_k/s_0)v_{\text{fs}}(\theta)$, where s_0 is the average shape change speed of the training data. The shape velocity model would predict that a body changing its shape twice as fast on average would move at double the body velocity at every phase. As a baseline model for comparing to all three models (to calculated RMSE_0), we used the constant mean speed model.

Averaged Analysis and Frequency Independence. Principally kinematic motion has profound implications on average behavior over a gait cycle. In particular, it provides that the net body motion over a cycle is independent of the speed with which that cycle of shape changes was executed. This property provides additional ways to operationalize a hypothesis test for principally kinematic motion. It is also of independent interest because when it holds, it signifies a reduction in the complexity of motion planning—each cycle can be taken to produce a single, characteristic rotation and translation, irrespective of speed. For example, such frequency independence has been observed in prior experiments on walking, slithering, and swimming animals and robots and has been important in analysis and design of locomotion gaits for theses systems (9, 15, 29–31).

Averaged analysis of principally kinematic motion is statistically straightforward. The net change in position and orientation of the legged system throughout a motion cycle is only minimally influenced by the cycle frequency or rate of the body shape change if the system is principally kinematic.

Results and Discussion

Instantaneous Principally Kinematic Modeling of Ant Walking. To test whether walking in small insects can be accurately modeled by principally kinematic equations, we tracked the distal limbs (tarsi) and body orientation of Argentine ants foraging freely along a flat substrate (Fig. 2). Based on the positioning and movement of the tarsi relative to the body center, we transformed the data from a time series to being based on stride phase, allowing us to correlate relative limb motion to body speed and body turning relative to the world frame. Consistent with prior work on the same dataset (3), we find that stride frequency is a stronger indicator of speed than stride length.[‡] Further, by comparing leg trajectories across phase between fast-straight and slow-straight walking (in Fig. 2*F*), we observe that leg motions largely resemble each other, demonstrating an independence of speed. That the limbs trace the same patterns across speeds suggests that inertia minimally contributes to ant walking, consistent with other principally kinematic regimes (50).

Our main results for ants are summarized in Fig. 3*A*. While the predictions of forward speed had similar accuracy between the shape velocity and principally kinematic models, only the principally kinematic model predicted turning velocity (average 55.5% vs. 0.0% for phase models and 1.1% for shape velocity models on straight-medium speed walking). The data-driven principally kinematic model surpassed the shape velocity model in its ability to predict speed and was the only model to provide any predictive information about turning. The principally kinematic model predicted behaviors that it had not been trained on, including left and right turning and slower and faster walking.

In ants we observe a fairly similar predictive ability with regard to forward speed for the shape velocity model and the principally kinematic model. We also found that ants hardly slip (having a 4.7% slip ratio) and that they follow similar motions at all speeds (*SI Appendix*, Figs. S2 and S3). Together these suggest that ants are principally kinematic because they are piecewise holonomic. Because the training data were for moderate speed with (on average) no turning, the phase model and the shape velocity model were entirely unable to predict the instantaneous turning rate. However, they were still able to predict some of the variability in forward velocity. The principally kinematic model could extrapolate from the variability in the training data and correctly predict the turning rate in all nine behavior categories.

Instantaneous Principally Kinematic Modeling of BigANT. That ant walking can be better modeled by principally kinematic models is not surprising, given their continuous contact with the ground using at least three limbs and evidence of limited slipping (4.7% slip ratio, see Fig. 1). To further test the application of principally kinematic motion to walking, we next examined the hexapedal robot BigANT performing turning walking behaviors (Fig. 3*B*) (53, 54). When the robot turns, the feet continuously slip against the ground (20% slip ratio for a 23° heading change per cycle, see Fig. 1), enabling us to test whether the principally kinematic model is effective for legged slipping.

As observed for ant walking, BigANT undergoes the same shape changes at all speeds (*SI Appendix*, Fig. S9), making the

[‡]We took the Bhattacharyya distance between the normal distributions of fast and slow foot position as a function of phase, yielding 0.38 ± 0.05 (taken at 100 evenly distributed phase samples including data over an eighth of a cycle), while the same distance on the foot velocity distributions yielded 0.66 ± 0.08.

Downloaded from https://www.pnas.org by UNIVERSITY OF CALIFORNIA DIGITAL LIBRARY CDL ACQUISITIONS GEISEL LIBRARY on September 12, 2022 from IP address 128.54.25.186.

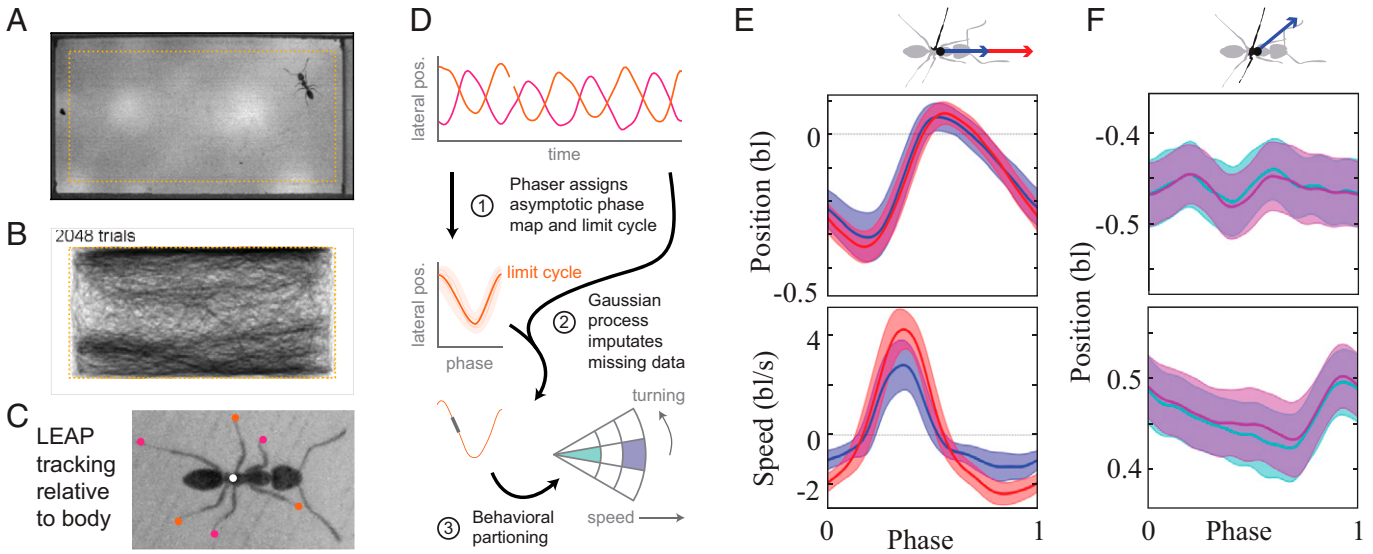

Fig. 2. We (*A*) captured ant motions in an arena and (*B*) logged the paths traced by the ants, including (*C*) points on the body (white) as well as the locations of their feet (red). (*D*) We detected these points using a deep learning network, which missed the locations of feet in some frames (e.g., step 1). We obtained an initial phase estimate from the detected feet and used frames with all feet observed to construct a Gaussian process with a periodic kernel, which we then used to impute the missing foot data (step 2). We partitioned the data into behavioral categories based on speed and turning rate (step 3). We performed a variety of sanity checks on the data, verifying commonly known facts. (*E*) (*Top*) When comparing slow (second quartile) and fast (top quartile) walking speeds, the instantaneous speed of middle legs changes (*Bottom*), showing that while the shapes remain the same (*Top*), the rate at which the ant goes through these shapes is variable. (*F*) As expected, ant turning is bilaterally symmetric; e.g., the middle leg fore-aft position when turning left (pink; solid line, mean; colored band, SD; units of body length) closely matched that when turning right (cyan; reflected and shifted 1/2 cycle).

hypothesis of principally kinematic behavior testable with these data. Surprisingly, the data-driven principally kinematic model performed dramatically better than the alternative models across every behavioral category. However, the principally kinematic model deteriorated when predicting forward speed while turning, and turning speed while forward speed was changed; i.e., it did a bit worse predicting the interaction of turning and speed change than it did with just one change or the other change.

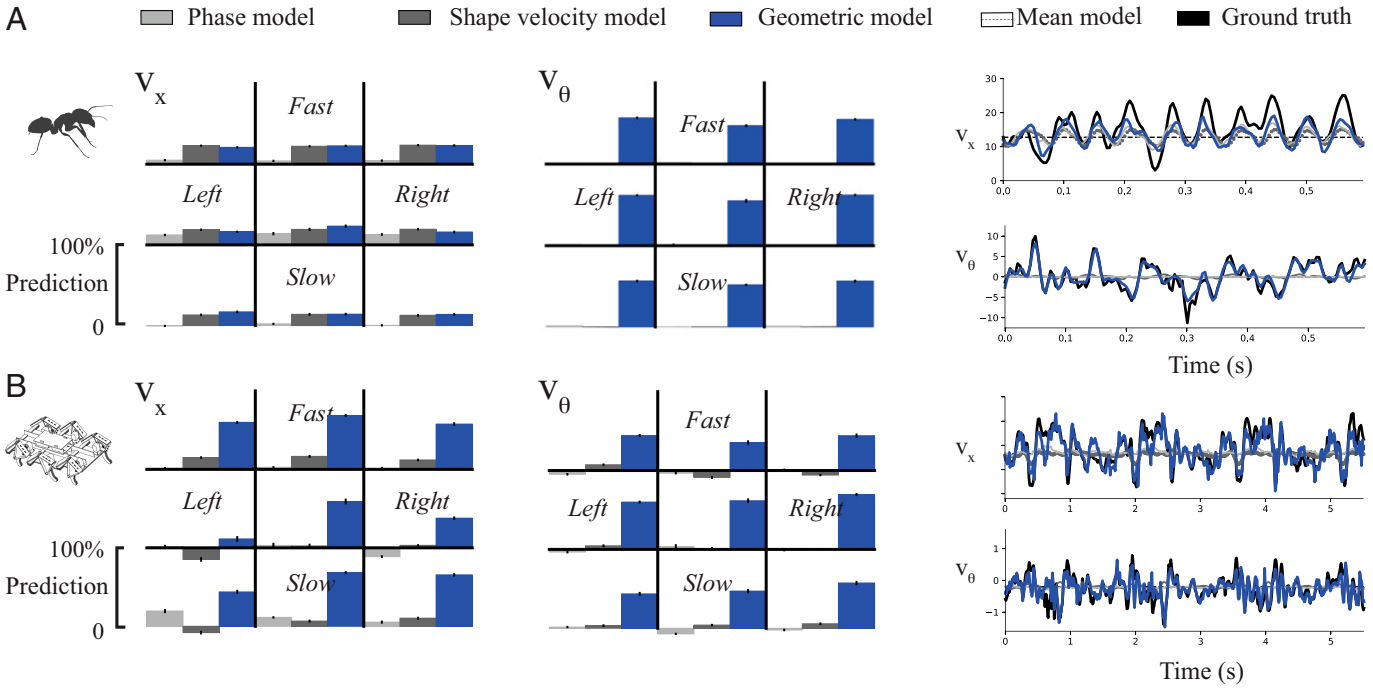

Fig. 3. Predictive value of data-driven principally kinematic models for ants and BigANT robots. We estimated our three models: phase only (light gray), shape velocity (dark gray), and data-driven principally kinematic (geometric model following ref. 24; teal). We trained the models on the middle speed with midrange turning behavior data (3rd quartile speed, middle tertile turning rate). We performed the same analysis on (*A*) ants, which turn both right and left, and (*B*) BigANT robots, which turn right at three different rates. We show the prediction quality of forward velocity V_x (*Left*) and turning rate V_θ (*Middle*) for all nine behavior categories with speed outside the lowest quartile. We also plotted illustrative, randomly selected time segments of the predicted variables (black) with all model predictions superposed (*Right*). For the piecewise holonomic, nonslipping ants, the shape velocity and principally kinematic models are almost equally good at predicting forward speed, but only the principally kinematic model was able to predict turning. The BigANTs were already turning, and mere shape velocity rescaling did far more poorly predicting their motion. The principally kinematic model came close to perfect prediction for the effect of speed changes on forward velocity and for the effect of increasing of decreasing turning at the same forward speed. It did somewhat more poorly predicting the motions in behaviors where both turning rate and forward speed were different.

Downloaded from https://www.pnas.org by UNIVERSITY OF CALIFORNIA DIGITAL LIBRARY CDL ACQUISITIONS GEISEL LIBRARY on September 12, 2022 from IP address 128.54.25.186.

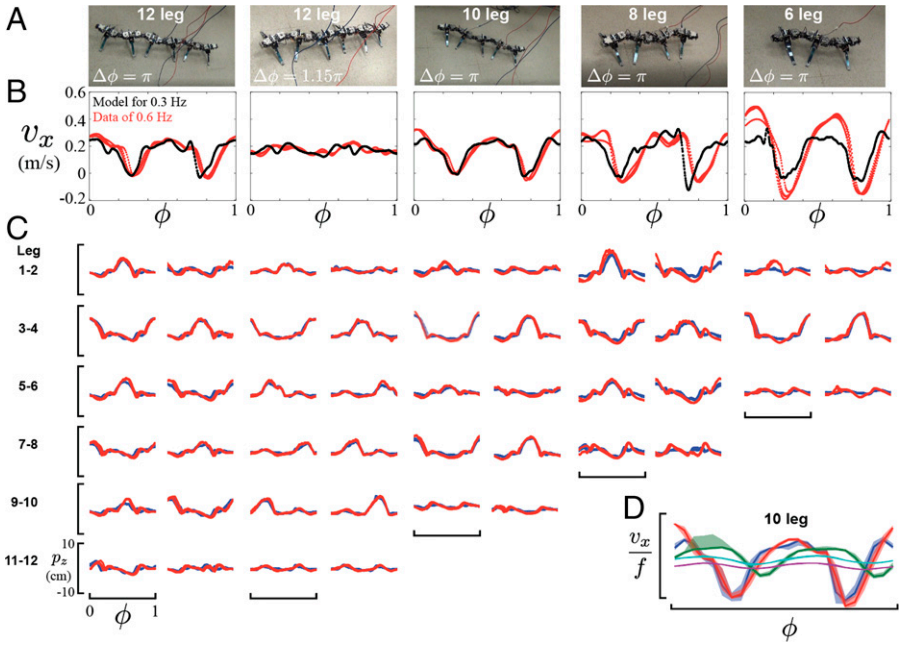

Fig. 4. Instantaneous analysis for the Multipods. (*A*–*C*) We show the 12-legged Multipod with two different gaits and the 10-, 8-, and 6-legged Multipods (columns from left to right). (*D*) As an illustrative example of the variability of outcomes, we plotted the frequency normalized forward velocity (v_x/f) as a function of phase for the 10-leg Multipod at gait frequencies (in Hz; solid line, mean; $\pm 35\%$, ribbon): 0.3 (blue), 0.6 (red), 1.2 (green), 2.4 (cyan), and 3.0 (magenta). The plot shows that the two lowest frequencies produce very consistent motion profiles, the two highest frequencies produce a different but consistent motion profile, and the 1.2 Hz motion is different from both. We examined the motion at the two lowest frequencies and here show the alternating gaits ($\Delta\phi = \pi$), where consecutive segments are in antiphase (first, third, fourth, and fifth columns). For comparison, we also show a nonalternating 12-legged gait (second column; $\Delta\phi = 1.15\pi$ between consecutive segments). To demonstrate the power of instantaneous principally kinematic modeling, we fit a principally kinematic model to the 0.3 Hz data (*B*, black) and used it to predict the observed motion at 0.6 Hz (*B*, red). The RMSEs of the prediction (*B*, left to right) are 0.055, 0.030, 0.041, 0.118, 0.133 m/s. Taken together, these results show that at low gait frequencies the Multipods undergo the same shape sequences (*C*) and that when they do, the instantaneous principally kinematic model predicts the body velocity quite well. This observation holds for different gaits (first vs. second column) and seems to hold better for morphologies with more rather than fewer legs.

While it might initially seem surprising that the phase-dependent velocity model does so poorly at predicting the very data on which it was trained (the middle tertile of turning and third quartile of speed), this result can be understood by the fact that our BigANT gait was designed to have a fairly constant forward speed. As a consequence, the phase-dependent velocity model is almost no better than the mean velocity model used as a baseline. On the other hand, the principally kinematic model does a good job of using the shape of the body to model the fluctuations around this mean velocity.

Analysis of the Multipod Robots.

Instantaneous analysis of Multipod. To test whether principally kinematic modeling of a slipping robot generalizes to other leg configurations and gaits we analyzed the motion of the Multipod robots, a family of multilegged robots that ranged in leg number from 6 to 12 legs (55, 56). The Multipod robots we used are shown in Fig. 4*A*, and a full description of their mechanics can be found in ref. 37, chap. 2.3. The Multipods raise an important issue—with their passive spring legs, Multipods might occupy a different part of their shape space when they move at different speeds. This is because even when friction with the environment removes all the inertial effects from the motion of the robot as a whole (captured in the g dynamics), inertial effects can influence the shapes (captured in the r trajectories). In analyzing our Multipod data we found that for each gait (choice of intersegmental phase offset $\Delta\phi$) and morphology, the body shapes expressed were consistent for the two lower frequencies (0.3 and 0.6 Hz), consistent but different for the two higher frequencies (2.4 and 3.0 Hz), and vastly different for 1.2 Hz (see *SI Appendix*, Fig. S12 for an illustrative example). The nonlinear dependence of the connection $A(r)$ on shape r implies that across gaits that occupy dissimilar shapes, as was the case between low and high frequencies in Multipod, we could not test the instantaneous principally kinematic property.

Averaged analysis of Multipod. Our results of such an averaged analysis, over all 520 morphology, gait, and frequency combinations, are summarized in Fig. 5. Our results reveal an averaged behavior that exhibits strong principally kinematic qualities—all morphologies and all frequencies fall within a master curve that depends on gait. The effect of frequency is almost unnoticeable in the range 0.3 to 2.4 Hz, and even at our maximal achievable $\times 10$ speed-up, the change in distance traveled per cycle is approximately 20%. While the instantaneous analysis showed that at different frequencies the details of the body velocity as a function of phase changed, this variability cancelled out across a cycle to produce average principally kinematic behavior. For purposes of planning, it seems it is safe to assume that a cycle of shape change will always produce the same motion through the world.

That the results are independent of leg number might seem surprising at first. However, principally kinematic motion is quasistatic. This suggests the following interpretation of our results. When a portion of the body is large enough to be principally kinematic on its own, it is inertial in the sense of being subject to net zero forces and torques. If several such body parts move in tandem, it would not matter whether they were connected to each other or not. Thus, a longer Multipod is in essence a convoy of shorter Multipods and falls on the same curve as its parts.

Constant Velocity Gaits Generalize Geometrically. The principally kinematic reconstruction equation $v_b = A(r)\dot{r}$ arises when the contact forces are so large compared to body inertia that the group momentum decays almost instantaneously (20, 25). A special case of this occurs when $v = \text{const}$. In that case it can be shown

Downloaded from https://www.pnas.org by UNIVERSITY OF CALIFORNIA DIGITAL LIBRARY CDL ACQUISITIONS GEISEL LIBRARY on September 12, 2022 from IP address 128.54.25.186.

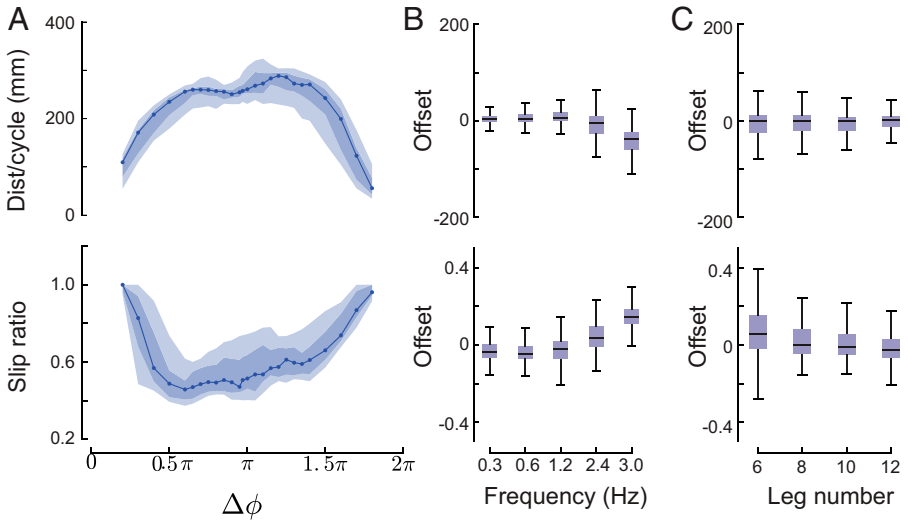

Fig. 5. Summary of $N = 520$ Multipod motion experiments with different gaits (phase offset $\Delta\phi$ between consecutive segments; $N_{\Delta\phi} = 26$), morphologies (number of leg segments 3 . . . 6), and gait frequencies (0.3, 0.6, 1.2, 2.4, and 3.0 Hz). We examine (*Top*) distance traveled per cycle and (*Bottom*) slip ratio, the distance a foot slipped over total foot travel. (*A*) All the experiments fell within a narrow band (solid line with points, median; dark ribbon, ±25%; and lighter ribbon, ±45%). After subtracting the effect of gait choice, we plotted the offset produced by (*B*) frequency and (*C*) morphology. Results show that until the highest frequency is reached, all the Multipod robots, over a range of ×8 in frequency and doubling in leg number, fall on a single curve, which is frequency independent and thus principally kinematic on average.

(*SI Appendix*, section 4) that for a variety of types of contact friction, as long as all contacts use the same type of friction, time-rescaling the body shape change would produce a geometrically identical motion at a rescaled speed. The implication of this observation is that if an animal or robot managed to discover a pattern of shape changes, $r(t)$, which produces a constant v, that pattern could be used for all magnitudes of v. The limiting factor would not be interaction with the environment; it would be the ability of the body to execute $r(st)$ at the speed rescaled by s. The principally kinematic reconstruction equation $v_b = A(r)\dot{r}$ arises when the contact forces are so large compared to body inertia that the group momentum decays almost instantaneously (25).

Conclusion

In this work we propose that legged locomotion in continuous contact regimes yields principally kinematic motion independent of whether feet remain in static contact or slip. We demonstrated this result through analysis of experimental data from walking ants, the hexapedal robot BigANT, and the Multipod family of multilegged robots with leg numbers from 6 to 12. While we have demonstrated effective tools for constructing data-driven models of periodic locomotion gaits in the principally kinematic regimes, there is much room for improvement: better tools for model fitting, methods to exploit piecewise holonomic structures where they exist, models with underactuation (the topic of another publication), and models with low dimensional group momentum.

We have shown that walking now falls within a broader class of principally kinematic locomotion which includes low Reynolds number swimmers such as small microorganisms (13), the slithering locomotion of snakes and limbless reptiles on hard ground (16), and the locomotion on (15, 29) and within granular material (9). This suggests a more sweeping hypothesis. Since principally kinematic movement is so prevalent among small animals, which are the majority of extant animals, and the ancestral form of larger animals, 1) the motor control and motor learning of animals large and small might be ancestrally adapted to learn principally kinematic movement, 2) animals would preferentially learn near-constant velocity gaits since those generalize geometrically to a large range of speeds, and 3) motor learning of more dynamical movements is done as a correction on top of a principally kinematic approximation, with the learning of principally kinematic motion as its core.

Centralized circuits that control cyclic limb movements are ubiquitous across walkers from ventral nerve cord ganglia in arthropods to central pattern generators in vertebrates. Hemichordates and vertebrates share similar motor-neuron architectures (38) pushing this similarity back to Deutrostomia, and vertebrates and arthropods share much of the patterning of the nervous system as well (39), suggesting an urbilaterian origin for much of the control of locomotion. This last common ancestor of bilateral animals—the urbilaterian—is currently presented as similar to modern planarians: a small, worm-like creature that swam or moved through the bed of bodies of water at slow speeds. As such, it was moving at low Reynolds numbers and was therefore approximately or fully principally kinematic. Our work here shows that if urbilaterian motor control could handle the relatively simple learning needed to optimize principally kinematic gaits (24), this capability would suffice throughout evolutionary history up to and including arthoropods' transition to land. While vertebrates grew large enough in the water to no longer be principally kinematic, the vertebrate transition to land would have brought them back into a principally kinematic regime—crawling through mud—where reliance on this ancestral mode of motor learning and control would have served them well. We suggest the hypothesis that all bilaterian motor control and learning, including that of vertebrates such as ourselves, is first and foremost geared for principally kinematic motion, learning to account for the effects of momentum later.

Navigation for animals is also greatly simplified in principally kinematic motion regimes since position with respect to the environment is determined by integrating body shape change. The use of step-counting (odometry) to inform travel distance has been observed in numerous species, including spiders (40), crabs (41), mantis shrimp (42), humans (43), rodents (44), and particularly desert ants (45). This path integration is somewhat trivial in the case of nonslip walking, as in the case of desert ants (46). However, path integration has also been observed under more challenging circumstances, including those that may induce slipping, such as desert ants walking up and down inclines (47). If walking was

Downloaded from https://www.pnas.org by UNIVERSITY OF CALIFORNIA DIGITAL LIBRARY CDL ACQUISITIONS GEISEL LIBRARY on September 12, 2022 from IP address 128.54.25.186.

not principally kinematic, odometry would not provide accurate travel information. Although animals may override odometry-based path integration using other cues (e.g., visual landmarks and chemical signals), the prevalence of odometry across animals demonstrates the potential functionality of principally kinematic walking and supports its broad applicability.

Our finding that principally kinematic motion applies to walking, even with slipping, will allow engineers and scientists to construct reduced complexity models of the physics of locomotion and generate control algorithms for movement. Most robotic control systems rely on simulations that incorporate dynamics such as in Gazebo (48), Bullet,[§] Mujoco,[¶] and Pinocchio (49). While the performance of these packages continues to improve, their simulations are often computationally heavy. Alternatively, principally kinematic models of locomotion are relatively simple, reducing both control design complexity and processing times. Given our findings that walking systems are well characterized by principally kinematic models, the use of these models for real-time robotic control may transform the development of legged robotics. This may be particularly beneficial when considering multilegged slipping, a domain where most dynamic simulations perform poorly or rely on machine learning to provide corrections which have no direct basis in physics.

In conclusion, principally kinematic motion is a unifying framework across swimming, burrowing, slithering, and now continuous-contact walking. Principally kinematic motion drastically reduces the complexity of modeling movement through the world and may have important implications for understanding the evolution of motor control and animal navigation, as well as informing streamlined robotic simulations and actuator controls.

Materials and Methods

We collected motion data from both ants and robots. All the motion data were collected using optical tracking. Most of the figures in this paper can be directly reproduced using the dataset and code at DOI: 10.7302/gqk6-3x41 (50).

Experimental Data Collection in Ants. We collected ant data using high-speed video recordings (FLIR Blackfly S cameras, at 240 fps) of ant workers foraging from overhead views as they walked across flat substrates. A comprehensive overview of the method can be found in ref. 3. Briefly, we trained a deep-learning based automated tracking algorithm (51) using a manually tracked subset of the data (679 frames) and used it to detect 10 body landmarks, including mouth, neck, and foot (tarsus) positions. In total, we analyzed 697,501 frames corresponding to 1.61 h of footage. We encoded the body frame locations of each ant as a homogenous matrix, g, computed from the x, y, and θ that the automated tracking obtained for the position and orientation of the body frame. We took the ant shape, $r \in \mathcal{Q}$, as a tuple of 12 numbers corresponding to the xy coordinates of the feet relative to the g coordinate frame. A total of 491,095 frames had one or more missing feet, and 35.7% of foot measurements were missing. We imputed foot locations using a periodic Gaussian process kernel, allowing us to discard only 63.4% of the frames for missing feet. We differentiated both r and g by taking the average of forward and backward finite differences to obtain $\dot{r}$ and the instantaneous body velocity $g^{-1}\dot{g}$, which we used to obtain v_x along the body, v_y across the body, and v_θ the turning rate. Further details about the animal tracking and foot imputation are provided in *SI Appendix*, *Detailed Materials and Methods–Ant tracking*.

Experimental Data Collection in Robots. For the robots, we used a commercial three-dimensional (3D) passive marker tracking system (10 Qualisys Oqus-310+ cameras at 120 fps, running QTM 2.17 build 4,000, interfaced to custom SciPy 0.17.0 code using the Qualisys 1.9 Realtime API) to track body orientation and limb motion.

Methods for BigANT robots. The BigANT robots are built from rigid foam board that is cut and folded along lines to form rigid structures and flexible joints, using the PARF methodology (52). Each leg of a BigANT is controlled by a single servo motor (Robotis Dynamixel MX64) in continuous rotation, and the leg sweeps through a stance and swing cycle through a kinematic linkage. To track the shape of a BigANT we recorded the commanded angles of all the servos, the 3D locations of 3 markers on each of its legs, and the locations of 11 markers spread across the body chassis. We verified that the servo angles predicted the leg position relative to the chassis to within close to measurement error; i.e., the legs moved rigidly (*SI Appendix*, Fig. S9). Thus, the coordinate frame of the chassis $g \in \mathrm{SE}(3)$, together with the servo angles r, provides a complete configuration space for the robot.

Our BigANT data came from three BigANT robots, executing a steering motion in a low, medium, or high turning rate at gait frequencies of 0.10 Hz through 0.34 Hz (*SI Appendix*, Fig. S7), We partitioned these data into nine behavior categories based on low, medium, and high turning rate and low, medium, and high forward speed. Together these categories contained left-turning high speed (3,598 points), no-turning high speed (2,183 points), right-turning high speed (1,458 points), left-turning medium speed (2,125 points), no-turning medium speed (2,544 points), right-turning medium speed (2,647 points), left-turning slow speed (1,510 points), no-turning slow speed (2,467 points), and right-turning slow speed (2,620 points). Our BigANT data are available in raw form at DOI: 10.7302/024q-kk06 (53) and processed (ready to use) form at DOI: 10.7302/jh82-fh69 (54).

Methods for Multipod robots. The Multipod family of robots each consists of three to six segments. Each segment contains two backbone motors (Robotis Dynamixel RX64) and a leg roll motor (Robotic Dynamixel MX106) which is attached to two spring-steel legs (ref. 37, chap. 2.3). Each segment was instrumented with motion tracking markers on the axes of the backbone motors, on the output of the roll motor, and at the tips of the spring legs. This allowed us to fully track the shape of the backbone and motor outputs and also observe the deflection of each individual spring leg.

We built Multipod robots with three, four, five, and six segments. Each of these we ran at five gait frequencies, 0.3, 0.6, 1.3, 2.6, and 3.0 (Hz), and each of those at multiple gaits was defined by taking the phase offset between the motion of consecutive segments to be one of 26 values between 0 and 2π. In total, this dataset consists of 520 trials, of at least four motion cycles in each direction for each robot; it is available in raw form at DOI: 10.7302/m05a-0d90 (55) and processed (ready to use) form at DOI: 10.7302/0fpj-dz57 (56).

Details of principally kinematic model fitting. Given timestamped data of shape, shape velocity, and body velocity for an animal or robot behavior, we are able to build a local principally kinematic model. Using an algorithm called Phaser, the data are mapped to the general form of an oscillator having dimension the size of the dimension of the shape. This algorithm computes an asymptotic phase for each time sample, which allows each data point of the behavioral data to be associated with a fraction of a cycle for that behavior. Using that information, an average behavior can be computed from the data by fitting a Fourier series to the shape data with respect to asymptotic phase. At this point, each data point is binned into fractions of the cycle, and a regression is computed fitting shape and shape velocity to body velocity. The regression terms are the change in shape from the average shape at that phase, the change in shape velocity from the average shape velocity at that phase, and all cross terms of the aforementioned terms. These regression coefficients are then fit as a function of phase across the phase bins, providing a single local model by which shape, shape velocity, and inputs can be sampled (in the neighborhood of the data collected) to yield predicted body velocity outputs.

Data, Materials, and Software Availability. Motion tracking data (CSV and GZ) and processing and plotting code (python 3, scipy, matplotlib) have been deposited in Deep Blue Data (DOI: 10.7302/gqk6-3x41, DOI: 10.7302/0fpj-dz57, DOI: 10.7302/m05a-0d90, DOI: 10.7302/jh82-fh69, and DOI: 10.7302/024q-kk06). Previously published data were used for this work (this work also uses data from DOI: 10.1098/rsos.192068).

[§] https://pybullet.org.

[¶] https://www.mujoco.org.

Downloaded from https://www.pnas.org by UNIVERSITY OF CALIFORNIA DIGITAL LIBRARY CDL ACQUISITIONS GEISEL LIBRARY on September 12, 2022 from IP address 128.54.25.186.

ACKNOWLEDGMENTS. We acknowledge Haotian Li for his work on Multipod. We acknowledge insightful conversations with Dan Goldman, Ross Hatton, and Howie Choset that emerged from the American Physical Society Robophysics conference. We also thank Andy Ruina, Matt Kvalheim, and George Council for their insightful conversations. The work of D.Z., B.B., and S.R. was funded in part by Army Research Office Defense University Research Instrumentation Program grant W911NF-17-1-0243, Army Research Office Multi University Research Initiative grant W911NF-17-1-0306, NSF Civil, Mechanical and Manufacturing Innovation grant 1825918, and the D. Dan and Betty Kahn Michigan–Israel Partnership for Research and Education Autonomous Systems Mega-Project. The work of N.G. is based upon work supported by the NSF under grant 2048235.

Author affiliations: [a]University of Michigan, Ann Arbor, MI 48109; [b]Department of Mechanical Engineering, University of Michigan, Ann Arbor, MI 48109; [c]Robotics Institute, University of Michigan, Ann Arbor, MI 48109; [d]Applied Physics Laboratory, Johns Hopkins University, Laurel, MD 20723; [e]Department of Biology, University of Portland, Portland, OR 97203; [f]Department of Mechanical and Aerospace Engineering, UC San Diego, San Diego, CA 92093; [g]Department of Ecology and Evolutionary Biology, University of Michigan, Ann Arbor, MI 48109; and [h]Department of Electrical and Computer Engineering, University of Michigan, Ann Arbor, MI 48109

1. R. M. N. Alexander, *Principles of Animal Locomotion* (Princeton University Press, 2003).
2. R. P. Kukillaya, P. J. Holmes, A hexapedal jointed-leg model for insect locomotion in the horizontal plane. *Biol. Cybern.* **97**, 379–395 (2007).
3. G. T. Clifton, D. Holway, N. Gravish, Uneven substrates constrain walking speed in ants through modulation of stride frequency more than stride length. *R. Soc. Open Sci.* **7**, 192068 (2020).
4. N. S. Szczecinski, T. Bockemühl, A. S. Chockley, A. Büschges, Static stability predicts the continuum of interleg coordination patterns in *Drosophila*. *J. Exp. Biol.* **221**, jeb189142 (2018).
5. S. Park *et al.*, Enhanced caenorhabditis elegans locomotion in a structured microfluidic environment. *PLoS One* **3**, e2550 (2008).
6. R. A. Merz, D. R. Edwards, Jointed setae–Their role in locomotion and gait transitions in polychaete worms. *J. Exp. Mar. Biol. Ecol.* **228**, 273–290 (1998).
7. S. M. Secor, B. C. Jayne, A. F. Bennett, Locomotor performance and energetic cost of sidewinding by the snake crotalus cerastes. *J. Exp. Biol.* **163**, 1–14 (1992).
8. B. C. Jayne, Kinematics of terrestrial snake locomotion. *Copeia* **1986**, 915–927 (1986).
9. R. D. Maladen, Y. Ding, C. Li, D. I. Goldman, Undulatory swimming in sand: Subsurface locomotion of the sandfish lizard. *Science* **325**, 314–318 (2009).
10. I. Jung, T. R. Powers, J. M. Valles Jr., Evidence for two extremes of ciliary motor response in a single swimming microorganism. *Biophys. J.* **106**, 106–113 (2014).
11. Y. Magariyama *et al.*, Simultaneous measurement of bacterial flagellar rotation rate and swimming speed. *Biophys. J.* **69**, 2154–2162 (1995).
12. S. D. Kelly, R. M. Murray, "The geometry and control of dissipative systems" in *Proceedings of 35th IEEE Conference on Decision and Control* (IEEE, Kobe, 1996), **Vol. 1**, pp. 981–986.
13. E. M. Purcell, Life at low Reynolds number. *Am. J. Phys.* **45**, 3–11 (1977).
14. A. Shapere, F. Wilczek, Geometry of self-propulsion at low Reynolds number. *J. Fluid Mech.* **198**, 557–585 (1989).
15. B. McInroe *et al.*, Tail use improves performance on soft substrates in models of early vertebrate land locomotors. *Science* **353**, 154–158 (2016).
16. H. C. Astley *et al.*, Surprising simplicities and syntheses in limbless self-propulsion in sand. *J. Exp. Biol.* **223**, jeb103564 (2020).
17. B. Chong *et al.*, Frequency modulation of body waves to improve performance of sidewinding robots. *Int. J. Robot. Res.* **40**, 1547–1562 (2021).
18. T. Wang *et al.*, "Generalized omega turn gait enables agile limbless robot turning in complex environments" in *Proceedings of 2022 International Conference on Robotics and Automation (ICRA)* (IEEE, Philadelphia, PA, 2022).
19. D. I. Goldman, D. L. Hu, Wiggling through the world: The mechanics of slithering locomotion depend on the surroundings. *Am. Sci.* **98**, 314–323 (2010).
20. J. M. Rieser *et al.*, Geometric phase and dimensionality reduction in locomoting living systems. arXiv:1906.11374 (26 June 2019).
21. R. L. Hatton, H. Choset, Geometric motion planning: The local connection, Stokes' theorem, and the importance of coordinate choice. *Int. J. Robot. Res.* **30**, 988–1014 (2011).
22. R. L. Hatton, H. Choset, Geometric swimming at low and high Reynolds numbers. *IEEE Trans. Robot.* **29**, 615–624 (2013).
23. S. Ramasamy, R. L. Hatton, "Soap-bubble optimization of gaits" in *Proceedings of 2016 IEEE 55th Conference on Decision and Control (CDC)* (IEEE, Las Vegas, NV, 2016), pp. 1056–1062.
24. B. A. Bittner, R. A. Hatton, S. Revzen, Geometrically optimal gaits: A data-driven approach. *Nonlinear Dyn.* **94**, 1933–1948 (2018).
25. M. D. Kvalheim, B. Bittner, S. Revzen, Gait modeling and optimization for the perturbed Stokes regime. *Nonlinear Dyn.* **97**, 2249–2270 (2019).
26. E. A. Shammas, H. Choset, A. A. Rizzi, Geometric motion planning analysis for two classes of underactuated mechanical systems. *Int. J. Robot. Res.* **26**, 1043–1073 (2007).
27. S. D. Kelly, R. M. Murray, Geometric phases and robotic locomotion. *J. Robot. Syst.* **12**, 417–431 (1995).
28. B. Goodwine, J. W. Burdick, Motion planning for kinematic stratified systems with application to quasi-static legged locomotion and finger gaiting. *IEEE Trans. Robot. Autom.* **18**, 209–222 (2002).
29. B. Chong *et al.*, Coordination of lateral body bending and leg movements for sprawled posture quadrupedal locomotion. *Int. J. Robot. Res.* **40**, 747–763 (2021).
30. Y. Ozkan-Aydin, B. Chong, E. Aydin, D. I. Goldman, "A systematic approach to creating terrain-capable hybrid soft/hard myriapod robots" in *Proceedings of 2020 3rd IEEE International Conference on Soft Robotics (RoboSoft)* (IEEE, New Haven, CT, 2020), pp. 156–163.
31. B. Chong, T. Wang, E. Erickson, P. J. Bergmann, D. I. Goldman, Coordinating tiny limbs and long bodies: Geometric mechanics of diverse undulatory lizard locomotion. *Proc. Natl. Acad. Sci. U.S.A.* **119**, e2118456119 (2022).
32. J. Ostrowski, J. Burdick, The geometric mechanics of undulatory robotic locomotion. *Int. J. Robot. Res.* **17**, 683–701 (1998).
33. J. P. Ostrowski, J. P. Desai, V. Kumar, Optimal gait selection for nonholonomic locomotion systems. *Int. J. Robot. Res.* **19**, 225–237 (2000).
34. J. Dai *et al.*, "Geometric swimming on a granular surface" in *Robotics* (Science and Systems, 2016).
35. B. Bittner, *PhD thesis*, Data-Driven Methods for Geometric Systems, University of Michigan (2020).
36. S. Revzen, J. M. Guckenheimer, Estimating the phase of synchronized oscillators. *Phys. Rev. E Stat. Nonlin. Soft Matter Phys.* **78**, 051907 (2008).
37. D. Zhao, *PhD thesis*, Locomotion of Low-DoF Multi-legged Robots, University of Michigan (2021).
38. A. M. Pani *et al.*, Ancient deuterostome origins of vertebrate brain signalling centres. *Nature* **483**, 289–294 (2012).
39. R. Lichtneckert, H. Reichert, Insights into the urbilaterian brain: Conserved genetic patterning mechanisms in insect and vertebrate brain development. *Heredity* **94**, 465–477 (2005).
40. E. A. Seyfarth, R. Hergenröder, H. Ebbes, F. G. Barth, Idiothetic orientation of a wandering spider: Compensation of detours and estimates of goal distance. *Behav. Ecol. Sociobiol.* **11**, 139–148 (1982).
41. M. L. Walls, J. E. Layne, Direct evidence for distance measurement via flexible stride integration in the fiddler crab. *Curr. Biol.* **19**, 25–29 (2009).
42. R. N. Patel, T. W. Cronin, Mantis shrimp navigate home using celestial and idiothetic path integration. *Curr. Biol.* **30**, 1981–1987.e3 (2020).
43. R. G. Golledge *et al.*, *Wayfinding Behavior: Cognitive Mapping and Other Spatial Processes* (JHU Press, 1999).
44. A. S. Etienne, R. Maurer, V. Séguinot, Path integration in mammals and its interaction with visual landmarks. *J. Exp. Biol.* **199**, 201–209 (1996).
45. H. Wolf, Odometry and insect navigation. *J. Exp. Biol.* **214**, 1629–1641 (2011).
46. R. Wehner, M. V. Srinivasan, "Path integration in insects" in *The Neurobiology of Spatial Behaviour*, K. J. Jeffrey, Ed. (Oxford University Press, 2003), pp. 9–30.
47. S. Wohlgemuth, B. Ronacher, R. Wehner, Ant odometry in the third dimension. *Nature* **411**, 795–798 (2001).
48. N. Koenig, A. Howard, "Design and use paradigms for gazebo, an open-source multi-robot simulator" in *Proceedings of IEEE/RSJ International Conference on Intelligent Robots and Systems* (IEEE, Sendai, Japan, 2004), pp. 2149–2154.
49. J. Carpentier *et al.*, "The Pinocchio C++ library–A fast and flexible implementation of rigid body dynamics algorithms and their analytical derivatives" in *Proceedings of International Symposium on System Integration (SII)* (IEEE, Paris, 2019).
50. BIRDS-Lab, *Walking Like a Worm: Dataset and Figures* (Deepblue Data Repository, 2021). Deposited 28 October 2021.
51. T. D. Pereira *et al.*, Fast animal pose estimation using deep neural networks. *Nat. Methods* **16**, 117–125 (2019).
52. I. Fitzner, Y. Sun, V. Sachdeva, S. Revzen, Rapidly prototyping robots: Using plates and reinforced flexures. *IEEE Robot. Autom. Mag.* **24**, 41–47 (2017).
53. BIRDS-Lab, *Bigant v6 Robot Motion Tracking Data–Raw Dataset* (Deepblue Data Repository, 2021). Deposited 30 August 2021.
54. BIRDS-Lab, *Bigant v6 Robot Motion Tracking Data–Processed Dataset* (Deepblue Data Repository, 2021). Deposited 30 August 2021.
55. BIRDS-Lab, *Birds Lab Multipod Robot Motion Tracking Data–Raw Dataset* (Deepblue Data Repository, 2021). Deposited 9 November 2021.
56. BIRDS-Lab, *Birds Lab Multipod Robot Motion Tracking Data–Processed Data and Code* (Deepblue Data Repository, 2021). Deposited 2 November 2021.

Downloaded from https://www.pnas.org by UNIVERSITY OF CALIFORNIA DIGITAL LIBRARY CDL ACQUISITIONS GEISEL LIBRARY on September 12, 2022 from IP address 128.54.25.186.